
Article:
Alzate-Cardona, J. D., Ruta, Sergiu Ionel, Chantrell, Roy William orcid.org/0000-0001-5410-5615 et al. (2 more authors) (2017) Surface anisotropy and particle size influence on hysteresis loops in La2/3Ca1/3MnO3 nanoparticles : A simulation approach. Journal of Magnetism and Magnetic Materials. pp. 451-458. ISSN 0304-8853

https://doi.org/10.1016/j.jmmm.2016.10.108

Surface anisotropy and particle size influence on hysteresis loops in $La_{2/3}Ca_{1/3}MnO_3$ nanoparticles: a simulation approach

J.D. Alzate-Cardona[1], S. Ruta[2], R.W. Chantrell[2],

O.D. Arbeláez-Echeverri[1], E. Restrepo-Parra[1]

[1]*Departamento de Física y Química,*

Universidad Nacional de Colombia,

Sede Manizales, A.A. 127 Manizales, Colombia.

[2]*Department of Physics, University of York,*

Heslington, York YO10 5DD, United Kingdom

Abstract

Thermal and hysteretic magnetic properties of $La_{2/3}Ca_{1/3}MnO_3$ nanoparticles were studied using Monte Carlo simulations, with emphasis on the influence of anisotropy. In this work, several nanoparticle sizes ranging from 2.32 nm to 11.58 nm were analyzed and their properties were compared to those of the bulk material. The magnetic behavior of the material was modeled using the three dimensional Heisenberg model with nearest neighbor interactions. Furthermore, both uniaxial and Néel anisotropies were considered for core and surface magnetic sites respectively. Deviations in the critical temperature and coercive field were observed for nanoparticles when compared with those of the bulk material. In addition to these properties, the special spin configurations that arise from the competition between the exchange, anisotropy and external magnetic field were also studied. All these effects are interpreted in terms of the surface properties such as the Néel anisotropy and the decrease in the coordination number.

I. INTRODUCTION

$La_{2/3}Ca_{1/3}MnO_3$ is one of the most studied magnetic compounds mainly because it has excellent magnetic and magnetotransport properties. In particular, it has a robust magnetoresistance, which is greater than that found in other magnetic materials such as magnetite and maghemite. Furthermore, it is straightforward to find compatible compounds of the family $La_xCa_{1-x}MnO_3$, that can present ferromagnetic, paramagnetic charge and orbital ordering simply by adjusting the stoichiometry, to build stable multilayers with excellent magnetotransport properties [1]. $La_{2/3}Ca_{1/3}MnO_3$ has also a strong chemical stability which make it easy to correlate the structural, electronic and magnetic properties when they are studied in a systematic way.

It has been recognized that the interesting properties of the compounds in the $La_xCa_{1-x}MnO_3$ family originate from the double exchange between $Mn^{3+} - O - Mn^{4+}$ [2, 3]. In these compounds, the double exchange mechanism explains the existence of ferromagnetism and metallic behavior at low temperatures. According to the double exchange model, the electrons can move between the manganese ions using oxygen, which is paramagnetic, as an intermediary. Consequently, the tunneling takes place between two manganese ions with different charge, thus interchanging their valence states ($Mn^{3+} - O - Mn^{4+} \rightarrow Mn^{4+} - O - Mn^{3+}$). When the proportion of lanthanum x is close to $1/3$ there is a maximum in the number of Mn^{3+} ions with one Mn^{4+} near neighbor, thereby maximizing the number of double exchange interactions. This is why $La_{2/3}Ca_{1/3}MnO_3$ has the highest Curie temperature and the best conductivity in this family; properties which justify special attention from the scientific community [4].

On the other hand, in any material, the surface properties are different from those in the bulk. Therefore, the properties of a material can be modified significantly when the relative amount of atoms in the surface is high; magnetic properties are not an exception. Surface effects are commonly linked to the lower coordination number of the surface atoms as well as the surface anisotropy, which arises from the broken symmetry in the surface, surface-core strains and magnetostriction [5]. Accordingly, surface effects become more important when the particle size decreases, specially when reaching the nanometric scale where the ratio of the number of atoms in the surface to the number of atoms in the core increases dramatically. Therefore, nanometric scale systems have potential for applications in magnetic memory

devices, sensors, medical treatments and catalysis [6, 7].

On the nanometric scale magnetic systems, surface effects manifest as low Curie temperature and low saturation magnetization compared with their bulk counterparts [8]. Those traits have attracted the interest of the scientific community for several years.

Kachkachi and Dimian studied the influence of the particle size and surface anisotropy in the hysteretic properties of spherical nanoparticles by means of the Landau Lifshitz equations [9]. Later, Kachkachi and Mahboub focused on the surface anisotropy and found that the Néel model was more realistic than a transverse anisotropy since it accounts for the loss of nearest neighbors in surface atoms [10]. Mazo-Zuluaga et al. studied the hysteretic properties of magnetite nanoparticles by means of Monte Carlo simulations; they considered nanoparticle sizes ranging from 2nm up to 7nm, considering different ratios of surface to core anisotropy. Their results reveal a strong influence of the sign and magnitude of the surface anisotropy on the coercive field [11].

Mahesh et al. performed experiments to study the effects of the particle size on the giant magnetoresistance in $La_{2/3}Ca_{1/3}MnO_3$. They concluded that the magnetoresistance decreases as the particle size increases [12]. Restrepo-Parra et al. studied the influence of the surface to volume ratio in the magnetic properties of $La_{2/3}Ca_{1/3}MnO_3$ nanoparticles using Monte Carlo simulations. They showed a direct correlation between the nanoparticle size and the critical temperature [13].

Although the magnetic properties of $La_{2/3}Ca_{1/3}MnO_3$ have been studied, deeper analysis is required on the influence of the anisotropy on the magnetic behavior. This work presents a comprehensive study of the influence of nanoparticle size and surface anisotropy in the thermal, magnetic and hysteretic properties of $La_{2/3}Ca_{1/3}MnO_3$ nanoparticles; furthermore, the effects of the surface anisotropy on the spins configuration in the low temperature regime are also investigated.

The rest of the work is organized as follows: section §II offers a description of the model, describing the constants, material structure and the Hamiltonian as well as the simulation technique, detailing the simulation parameters, observables and algorithms. Then, section §III presents the results and discussion of the static magnetic and hysteretic properties of manganite as well as some spin configurations exhibited by ferromagnetic materials with surface anisotropy are presented. Finally, section §IV contains the main conclusions and

remarks on this work.

II. MODEL AND SIMULATION

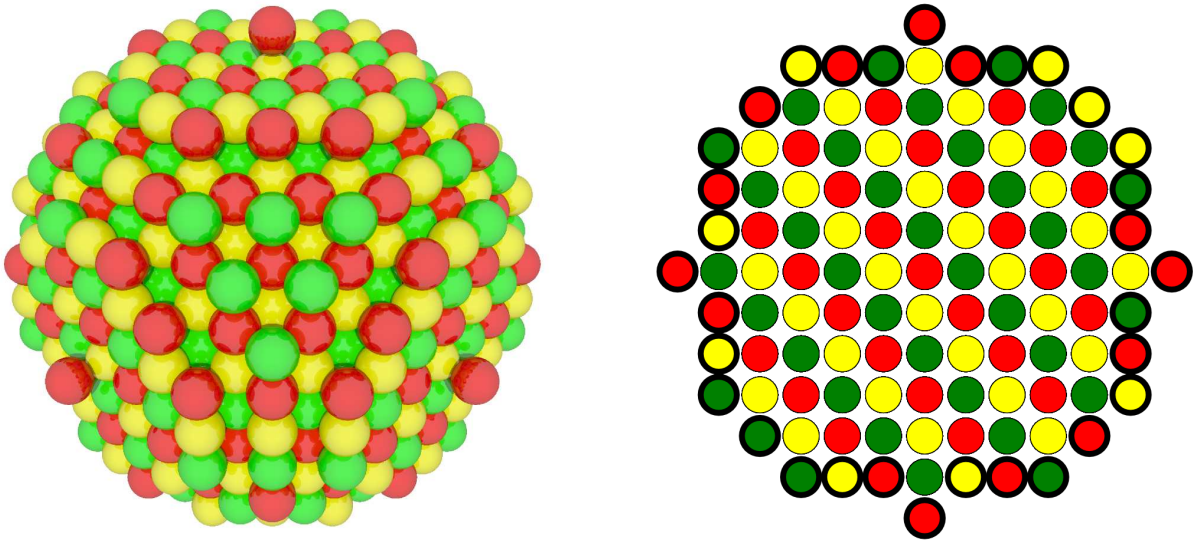

(a) (b)

Figure 1: (Color online) Schematic diagram of a $La_{2/3}Ca_{1/3}MnO_3$ nanoparticle in (a) three dimensional view and (b) cross section view, with a diameter of 12 ions. There are three types of ions: Mn^{4+d3} (red), Mn^{3+eg} (green) and $Mn^{3+eg'}$ (yellow). In the cross section view, the surface atoms are outlined in black.

The manganite $La_{2/3}Ca_{1/3}MnO_3$ is a ferromagnetic compound with a Curie temperature of 260 K. The compound has three types of magnetic ions, Mn^{4+d3} (with a spin $S = 3/2$) which bonds to Ca^{2+} ions, Mn^{3+eg} and $Mn^{3+eg'}$ (both with a spin $S = 2$), bonded to La^{3+} ions. Figure 1 shows a scheme of the magnetic ions in a 12 ion diameter manganite nanoparticle. The magnetic sites in this manganite organize themselves in a perovskite structure (a simple cubic lattice) with a coordination number of six, Hotta and Dagotto found that the magnetic sites are organized in the periodic fashion shown in figure 1 [14]. In a nanoparticle, the surface atoms lose some of their neighbors (dangling bonds); therefore, they end up with a

lower coordination number. Each of the magnetic sites are modeled with Heisenberg spins, whereas non magnetic ions (O, Ca and La) are left out of the simulation.

The magnetic behavior of the system is modeled with a Heisenberg Hamiltonian with nearest neighbor exchange interactions, magnetocrystalline uniaxial anisotropy and Néel's surface anisotropy.

$$\mathcal{H} = -\sum_{\langle i,j \rangle} J_{ij} \vec{S}_i \cdot \vec{S}_j - K_i \sum_i \left(\vec{S}_i \cdot \hat{n}_i \right)^2 - h \sum_i \vec{S}_i \cdot \hat{h} \tag{1}$$

where, $\langle ij \rangle$ means sum over the nearest neighbor pairs, J_{ij} is the exchange interaction constant between the sites labeled i and j, $\vec{S}_i$ and $\vec{S}_j$ are the spins of the magnetic sites labeled i and j, K_i is the anisotropy constant, $\hat{n}_i$ is the anisotropy axis, h is the applied field strength and $\hat{h}$ is a unit vector parallel to the applied field (this can be translated to energy units through the relation $H = {}^{h}/_{\mu}$, where μ is the magnetic moment of the Mn ions [15]).

Bond	$J\ \left[\text{meV} \cdot \text{link}^{-1}\right]$
Mn^{3+eg}-O-$Mn^{3+eg'}$	4.65
$Mn^{3+eg'}$-O-Mn^{4+d3}	1.35
Mn^{3+eg}-O-Mn^{4+d3}	7.77

Table I: Values for J considered in the different nearest neighbor pair types.

The values of J_{ij} were used in a per interaction type basis, as shown in table I. Those numerical values were fitted by Restrepo-Parra et al. to reproduce the Curie temperature of this manganite (~260 K) by adding a multiplicative factor to those found by Uhl and Siberchicot using density functional theory simulations [13, 16]. Similarly, the magnitude of the spin S_i in each site is assigned according to the type of ion as mentioned.

The anisotropy constant K_i takes the values K_c for ions within the core and K_s for surface ions. The value of K_c was fixed at $1.284\,\text{meV} \cdot \text{atom}^{-1}$, while K_s was treated as a simulation parameter via the variation of the ratio ${}^{K_s}/_{K_c}$; likewise, the anisotropy axis $\hat{n}_i$ takes the value

$\hat{e}_z$ (the canonical unit vector in the z direction) for the magnetic sites within the core, while

$$\hat{n}_i = \frac{\sum_{\langle j \rangle} \hat{e}_{ij}}{\left\| \sum_{\langle j \rangle} \hat{e}_{ij} \right\|} \tag{2}$$

where the sum runs over $\langle j \rangle$, i.e., the nearest neighbors of the site labeled i and $\hat{e}_{ij}$ is a unit vector parallel to the direction $\vec{r}_i - \vec{r}_j$.

Through the simulations in this study, the applied field direction $\hat{h}$ was held constant and parallel to the uniaxial anisotropy axis $\hat{e}_z$.

In order to compute the equilibrium magnetic properties, the Metropolis Monte Carlo algorithm was used in all the simulations. In each spin flip attempt, a random spin was drawn from a uniform distribution over the surface of a sphere. In order to calculate critical temperatures, a cooling down routine was used, whereas to compute the hysteretic properties, an hysteresis loop routine was used.

The cooling down routine consisted in taking the system from a high temperature, i.e., a temperature above T_C, down to a low temperature slightly above 0K with a small temperature step. The state of the system, given by the spin of each magnetic system, was initialized as random spin directions at high temperature. At each temperature step, the system was subjected to 5×10^5 Monte Carlo steps, of which the first 10^5 where taken to allow the system to reach thermal equilibrium.

The hysteresis loop routine consisted in taking the system from a random spin configuration with a negative saturating external applied field strength $-h_{sat}$, up to a positive saturating external applied field strength $+h_{sat}$, and then back to $-h_{sat}$, with a small and constant field step. In each step, the system was subjected to 1×10^5 Monte Carlo steps, and the first 2×10^4 were discarded to filter out the noise that would arise from the discrete applied field strength steps.

In both routines, the magnetization of the core and surface of the nanoparticle (total magnetization for the bulk) and the total energy of the spin configuration were recorded for each Monte Carlo step, even for those to be dropped later on in the analysis. Using this technique, the relaxation time and stability can be observed after the simulation and the number of time steps for relaxation can be established after the fact, thus, reducing the danger of having to repeat the simulation changing those parameters.

Diameter [ions]	Diameter [nm]	N [ions]
6	2.32	123
8	3.09	257
12	4.63	925
16	6.18	1209
20	7.72	4169
30	11.58	14147

Table II: Sizes of the simulated nanoparticles, associated with their total number of magnetic sites.

The sizes of the simulated nanoparticles ranged from 2.32 nm (6 ions in diameter) to 11.58 nm (30 ions in diameter), the diameter of the simulated systems in ions and nm as well as their total number of magnetic sites, are shown in table II. The properties of those nanoparticles were compared to the properties of a bulk material. For the simulated bulk material, we considered a cubic system with a linear size of 12 ions (4.63 nm) and $N = 1728$ magnetic sites. Furthermore, periodic boundary conditions were applied to the bulk system.

The surface anisotropy constant K_s was varied changing the surface to core anisotropy ratio ${}^{K_s}/_{K_c}$; this value was varied using powers of ten, and both positive and negative surface anisotropies were considered. The values of the ratios used follow the relationship $\log_{10}\left({}^{|K_s|}/_{K_c}\right) = \{0, 1, 2, 3, 4, 5\}$; therefore, $\pm K_s = 1, 10, 100, \ldots$ meV $\cdot$ atom^{-1} and so on.

From the stored time series, the normalized magnetization and susceptibility were computed. The magnetization was normalized to the maximum possible magnetization, that was calculated using the formula:

$$M_S = \sum_{\alpha} n_\alpha \left|\vec{S}_\alpha\right| \tag{3}$$

where the sum runs over the ion types α (Mn^{3+eg}, $Mn^{3+eg'}$ and Mn^{4+d3}), n_α is the number of ions of type α in the sample, and $\left|\vec{S}_\alpha\right|$ is the spin modulus of the ion of type α ($^3/_2$ for Mn^{3+eg},

2 for $Mn^{3+eg'}$ and Mn^{4+d3}). Then the magnetization is computed using a time average,

$$\langle M \rangle = \frac{1}{M_S} \sum_{t=N_{cut}}^{N_{max}} \left| \vec{M}_t \right| \tag{4}$$

where N_{cut} is the number of Monte Carlo steps required to achieve stability, N_{max} is the total number of Monte Carlo steps and $\vec{M}_t$ is the magnetization of the system at the time step t. The magnetization of the system was computed as the sum over all sites: $\vec{M}_t = \sum_i \vec{S}_i$. Furthermore, the susceptibility was evaluated using the formula:

$$\chi = \frac{1}{k_B T} \left[\langle M^2 \rangle - \langle M \rangle^2 \right] \tag{5}$$

where,

$$\langle M^2 \rangle = \frac{1}{M_S^2} \sum_{i=N_{cut}}^{N_{max}} \left| \vec{M}_i \right|^2 \tag{6}$$

The coercive field was estimated using linear regression applied to the points that cross the x-axis in the hysteresis loop. Then, the right and left coercive fields were evaluated. Moreover, the coercive field was estimated using the equation:

$$h_c = \frac{|h_{c,right}| + |h_{c,left}|}{2} \tag{7}$$

where $h_{c,rigth}$ and $h_{c,left}$ are the right and left coercive fields in the hysteresis loop.

III. RESULTS AND DISCUSSION

Figure 2a shows the normalized magnetization and susceptibility for a bulk system with a linear size of 21 ions. The peak value of the magnetic susceptibility, also shown in figure 2a, indicates a bulk critical temperature around 260 K, which is consistent with other theoretical and experimental results [17]. Furthermore, figure 2b shows the magnetization and susceptibility of two nanoparticle sizes. The curves for $D = 30$ ions show very good agreement with their bulk counterparts, with only a slight reduction of the critical temperature. The lower critical temperature can be attributed to finite size effects. For $D = 16$ ions the size effects accentuate, yielding an even lower critical temperature and a much less sharper susceptibility peak indicating a reduction on the criticality of the phase transition.

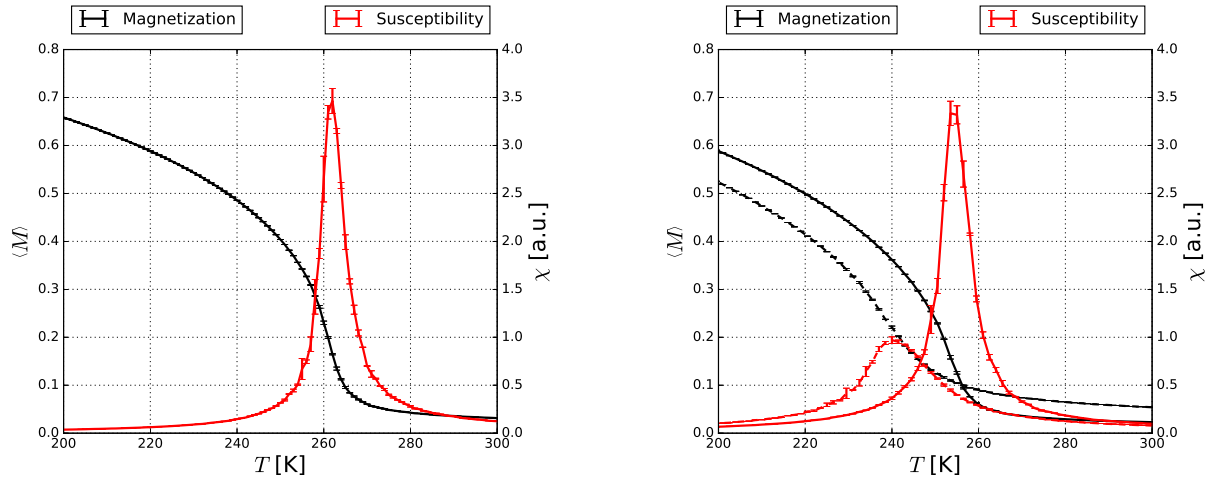

Figure 2: Critical temperature behavior of the bulk $La_{2/3}Ca_{1/3}MnO_3$ system as well as for nanoparticles. Magnetization and susceptibility for (a) bulk with a linear size of $L = 21$ ions and (b) a nanoparticles of diameter $D = 30$ ions (solid) and $D = 16$ ions (dashed) (lines are just a guide to the eye).

Figure 3a shows the critical temperature of $La_{2/3}Ca_{1/3}MnO_3$ nanoparticles as a function of their diameter. Results show a monotonic increase of the Curie temperature with the nanoparticle diameter, saturating at the bulk Curie temperature, $T_C = 260\,\mathrm{K}$. This behavior is usually attributed to finite size effects which include surface dominance at low diameters as well as lower average coordination number. As mentioned before the magnetic sites in the surface have a lower coordination number, as their relative population increases for smaller nanoparticles, the average coordination number decreases as well. With a lower average coordination, the magnetic bond density evidently decreases, and so does the amount of energy necessary to break the ferromagnetic ordering. Therefore, we observe a lower critical temperature as the diameter of the nanoparticles decrease. Similar results have been found by Velásquez et al. while studying the pseudocritical behavior of isolated ferromagnetic nanoparticles through the both the variational and Monte Carlo methods, and Iglesias and Labarta while studying the finite size effects on maghemite nanoparticles using Monte Carlo simulations [18, 19]. The surface to core dominance can be characterized using the ratio of the number of ions in the core to the number of ions of the surface, or N_c/N_s ratio. Figure

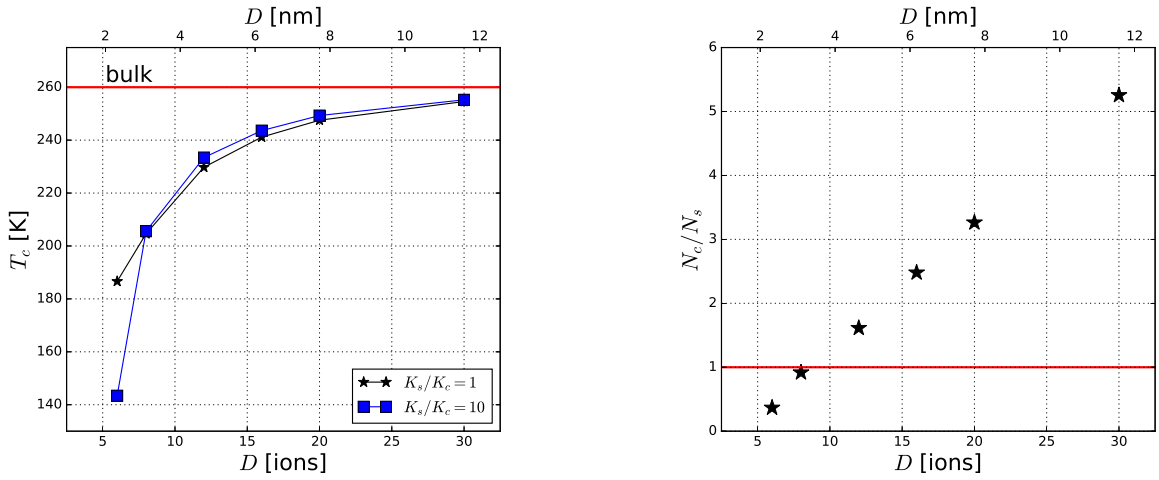

(a) (b)

Figure 3: (a) Critical temperature T_c as a function of the nanoparticle diameter and (b) dependence of the core to surface ratio, N_c/N_s, with the nanoparticle diameter, as a support figure (lines are just a guide to the eye).

3b, shows the value of the surface to core ratio for the simulated nanoparticles. Note that this ratio fits a linear trend because the number of ions in the core grows in proportion to the cube of the diameter whereas the number of atoms in the surface grows in proportion to the square of the diameter. The (red) horizontal line in figure 3b shows the threshold below which the number of ions on the core is lower than the number of ions in the surface and vice versa.

Figure 4a shows the hysteresis loops for different kinds of boundary conditions in the same bulk system. From the results one can readily appreciate that the coercive field of a bulk system with periodic boundary conditions (PBC) is considerably higher than that of the same system with free boundary conditions (FBC). Conversely, when free boundary conditions are applied instead of periodic boundary conditions, the hysteresis loop becomes significantly rounder. The dramatic change in the coercive field can be attributed to size effects which are induced once the boundary conditions are relaxed, whereas, the change in the squareness of the hysteresis loop can be attributed to both size effects and the surface anisotropy of the xz and yz facets of the cube that would be perpendicular to the applied field direction.

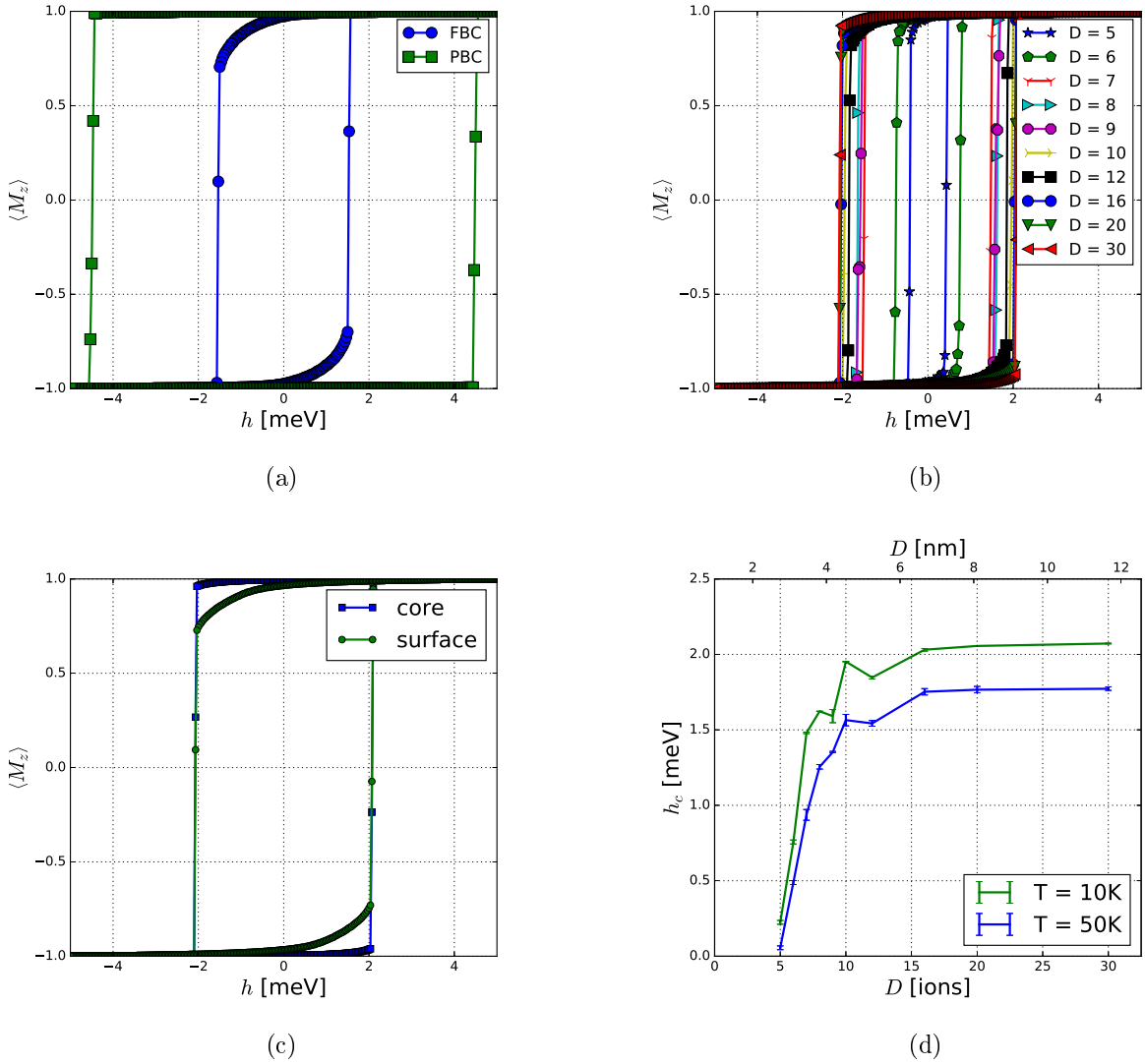

Figure 4: Hysteresis loops at $T = 10K$ and ${}^{K_s}/_{K_c} = 1$ for (a) bulk system using periodic boundary conditions and free boundary conditions with surface anisotropy, (b) several nanoparticle diameters and (c) core and surface of a nanoparticle with diameter $D = 30$ ions and, on the other hand, (d) coercive fields for different nanoparticle diameters at $T = 10K$ and $T = 50K$ (lines are just a guide to the eye).

As shown in figure 4b, with increasing diameter of the nanoparticles, their hysteresis loops widen and become more square; the increase in width is monotonic and saturates slightly above $h = 2\,\text{meV}$. The asymptotic value of the coercive field for the nanoparticles is, at most, half of the coercive field of the bulk system (periodic boundary conditions); on the other hand, this value is slightly greater than the coercive field of a large cubic system with

free boundary conditions and without surface anisotropy. To summarize, the coercive field of the nanoparticles saturates to a field bounded by the coercive field of a bulk system with free boundary conditions and boundary conditions, figure 4a.

The increase in squareness in the hysteresis loops with increasing nanoparticle diameter can be attributed to the increasing dominance of the core for bigger nanoparticles. As shown in figure 4c, in our simulations where the applied field is parallel to the uniaxial anisotropy axis of the core, the contribution of the core sites to the hysteresis loop is more square than the contribution from the surface as the anisotropy axes of the surface sites are evenly distributed in the range between parallel and perpendicular to the applied field direction. For this reason, as the diameter increases and so the $^{N_c}/_{N_s}$ ratio, the squared contribution to the hysteresis loop becomes dominant.

Figure 4d shows the dependence of the coercive field on the diameter. Results show a monotonic increase in the coercive field approaching an asymptotic value for particle sizes above $D = 4 \sim 5$ ions. Although we did not perform simulations below $D = 5$ ions due to the loss of stoichiometry, it is plausible to speculate that the coercive field would fall to zero below a diameter in the range between 3 and 5 ions. This result is consistent with the (super)paramagnetic and single domain regimes observed in experimental [20, 21] and theoretical [22] studies. Essentially, below a particle diameter d_0 (3 to 5 ions in this case) the system will be in a (super)paramagnetic regime, whereas above d_0 and below a critical diameter d_c (not reached in our simulations) the system will be in a single domain regime, where the normalized coercive field increases. Above d_c the system enters a multi domain regime where the normalized coercive field presents an exponential decrease. To observe this phenomenon, the magnetostatic interaction should be taken into account. See for instance, works by Kolhatkar et al., Sung Lee et al. and Yanes et al. in refs. [20–22].

Figure 5 shows the influence on the coercive field of increasing the positive surface anisotropy in a nanoparticle of $D = 12$ ions as a function of the temperature. Zianni et al. found a similar behavior for small magnetic nanoparticles, however their results, based on a strong crystalline anisotropy in the surface compared to the anisotropy in the core ($^{K_s}/_{K_c} = 10$), showed a more dramatic increase of the coercive field at low temperatures, overestimating the coercive field from experimental results in said low temperature region [23]. The curves

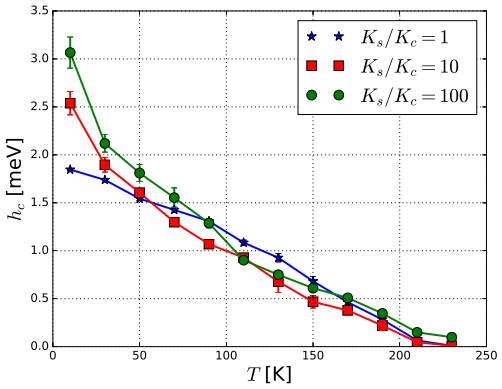

Figure 5: Temperature dependence of the coercive field for a nanoparticle with diameter $D = 12$ ions and ${}^{K_s}/_{K_c} = \{1, 10, 100\}$. The dashed lines are only a guide to the eye for a better visualization.

in figure 5 feature crossover points; this means that increasing the value of the positive surface anisotropy will increase, or decrease, the coercive field of a nanoparticle according to the temperature. This is an evidence of the complex temperature dependence of the non-uniformity of the magnetization. Furthermore, all of the curves, ${}^{K_s}/_{K_c} = 1$, ${}^{K_s}/_{K_c} = 10$ and ${}^{K_s}/_{K_c} = 100$, show a monotonic decrease of the coercive field; that is the expected behavior, since, as the temperature increases, the material tends to become paramagnetic with an implied coercive field of zero.

Figure 6a shows the dependence of the coercive field on the surface to core ratio ${}^{K_s}/_{K_c}$ for both positive and negative values at low temperature. In both cases, the coercive field tends to increase with ${}^{K_s}/_{K_c}$; however, for the positive, case the magnitude of the increase is greater. Furthermore, the curve for ${}^{K_s}/_{K_c} > 0$ exhibits large error bars; this can be attributed to the choice in the spin update policy and to different magnetization switching paths due to excessive strains in the surface. Iglesias and Labarta studied the influence of surface anisotropy on maghemite nanoparticles, and found a monotonic increase of the coercive field as the surface to core anisotropy ratio increased (only for ${}^{K_s}/_{K_c} > 0$). The results of ref [15] are consistent with ours up to ${}^{K_s}/_{K_c} = 100$ after which we find an apparent saturation. Figure 6b shows the dependence of the coercive field on the positive surface to core ratio for different temperatures. In this figure, we confirm that the impact of increasing

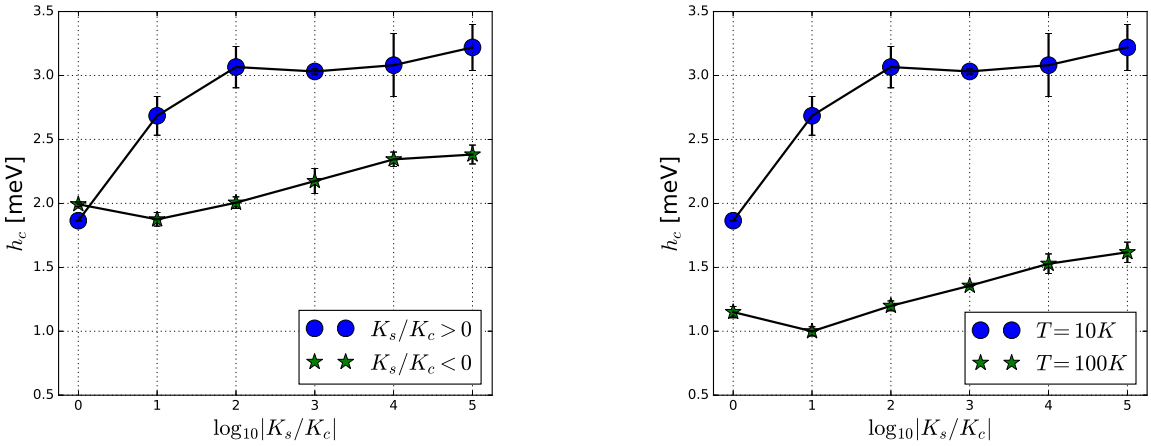

Figure 6: Coercive field as a function of $\log|{}^{K_s}/_{K_c}|$ for a nanoparticle with $D = 12$, for (a) different signs of the surface anisotropy constant at $T = 10\,\mathrm{K}$ and (b) different temperatures for a positive surface anisotropy constant (lines are just a guide to the eye).

the surface to core anisotropy ratio is modified heavily by the temperature. This is because the non-collinearity is reduced due to the thermal fluctuations.

The results shown in figure 6b are consistent with the ones shown in figure 5. Several features of6b are important to note at both $T = 10\,\mathrm{K}$ and $T = 100\,\mathrm{K}$. In the case of $T = 10\,\mathrm{K}$, there is a large step upwards in the coercive field between ${}^{K_s}/_{K_c} = 1$ to ${}^{K_s}/_{K_c} = 10$ and then a slightly smaller step upwards in the coercive field between ${}^{K_s}/_{K_c} = 10$ to ${}^{K_s}/_{K_c} = 100$ which can be readily confirmed in figure 6b by looking at the three first points of the coercive field curve for $T = 10\,\mathrm{K}$. Similarly for $T = 100\,\mathrm{K}$ there is a small steps decrease in the coercive field between ${}^{K_s}/_{K_c} = 1$ to ${}^{K_s}/_{K_c} = 10$ followed by a small step increase in the coercive field between ${}^{K_s}/_{K_c} = 10$ to ${}^{K_s}/_{K_c} = 100$, as can also be readily confirmed in figure 6b by investigation of the three first points of the coercive field curve for $T = 100\,\mathrm{K}$.

Figure 7 shows different spin configurations collected during a hysteresis loop, with the following parameters, ${}^{K_s}/_{K_c} = \pm 10000$ and $T = 10K$. We will discuss separately the positive and negative surface to core anisotropy cases. For ${}^{K_s}/_{K_c} = 10000$, the surface ions are blocked in the radial direction and only the top and bottom magnetic sites of the shell

can align to the applied magnetic field. In this case, depending on the external field, the spins can align in throttled states 7 (states A, C and D) or states between throttled and hedgehog (state B) with a magnetization close to zero. Furthermore, it is important to note that the differences between the states at B and C are concentrated in the surface to core interface. In the magnetic configuration at B the interface spins align with the local field from the shell and core, leading to maximum stability, whereas at point C the magnetostatic field dominates, maximizing the magnetization. The hysteresis loop for the positive surface to core anisotropy ratio features several jumps in magnetization. These jumps can be attributed to the entire or partial switching of the magnetization of the sites in the surface, due to the external field; it can be said that the spins on the surface would not change gradually but suddenly. Kachkachi and Dimian show similar hysteresis loops using the Néel model in a generic ferromagnetic material and solving the Landau-Lifshitz equations [9]. They recognize two kinds of point that characterize the hysteresis loops. The first is named the critical field, which marks the limit of meta-stability, and the second is called switching field, or coercive field, where the projection of the magnetization on the field direction changes sign.

On the other hand, when the ratio K_s/K_c is negative, the states of the surface spins are tangential to the surface. Therefore, there are not jumps in the hysteresis loops. In this case, all the states A, B, C and D show an artichoke configuration, and the poles of the artichoke move as the applied magnetic field varies. Furthermore, when transitioning from the state B to the state C, there are some interface spins that align with the applied field as well as the surface spins for B and only to the applied for C; however, those spins are not distributed in the sides of the nanoparticle (with respect to the applied field direction) but in the top and bottom of the nanoparticle. Beyond that, the states also present blocking but only in the top and bottom side of the nanoparticle where a couple of spins are blocked to be perpendicular to the applied magnetic field direction.

Regarding the anisotropy, figure 8 shows the possible spin configurations for different values of K_s/K_c at low temperature. When the surface anisotropy is negligible in comparison to the core anisotropy, the spins tend to orient in the same direction because of the exchange coupling, shown in figure 8 (a). When the positive surface anisotropy is high, the surface

spins are blocked radially, but the core spins take a direction such that they compensate the exchange coupling and the uniaxial anisotropy in the $\pm z$ direction, forming a "throttled" configuration, shown in figure 8 (b). As K_s becomes increasingly positive, the spins are blocked strongly normal to surface and they force to their neighbors to align with them, according to figure 8 (c). This causes a net magnetization equal to zero. Furthermore, they can be oriented either inward or outward direction, because this state is twofold degenerate [5]. When the surface anisotropy is negative, the surface spins are oriented in a direction tangential to the surface producing an "artichoke" configuration, as shown in figure 8 (d). These same configurations were found by Berger et al. [24], who studied the influence of strong surface anisotropy in ferromagnetic nanoparticles. Similarly, Mazo-Zuluaga et al. [11] studied the magnetic properties of magnetite nanoparticles and showed a strong difference between positive and negative surface anisotropy, also reporting configurations similar to those found in this work. All of the above effects are most significant in particles where the surface anisotropy is comparable to the exchange [5, 15, 25].

IV. CONCLUSIONS

The effect of the surface anisotropy and particle size on the hysteretic and magnetic behavior of manganite $La_{2/3}Ca_{1/3}MnO_3$ nanoparticles was studied. Monte Carlo method with Metropolis algorithm and three-dimensional classical Heisenberg model were used for modeling magnetic and hysteretic properties of nanoparticles of $La_{2/3}Ca_{1/3}MnO_3$. Magnetization and magnetic susceptibility per site were obtained for bulk material in order to reproduce the critical temperature. In the same way, critical temperatures for nanoparticles with different size was computed. A shift toward low temperatures of T_c was observed for decreasing nanoparticle size. This phenomenon is due to the lower number of ions on the surface than the core. Nevertheless, T_c tends toward the bulk transition temperature (260 K) with increasing nanoparticle diameter.. The equilibrium spin configuration at extreme values of K_s/K_c were shown.

Furthermore, the surface to core anisotropy ratio showed almost no influence on the critical temperature of manganite nanoparticles; however, for very small nanoparticles ($D = 5$ nm) the influence of the surface to core anisotropy ratio becomes significant.

Hysteresis loops of nanoparticles were obtaining varying the diameter and K_s/K_c. The diam-

eter has strong influence on the coercive field, due to the surface anisotropy and the ratio of the number of ions on the surface and the number of ions on the core.

The dependence of the coercive field on the temperature was computed for different values of ${}^{K_s}/_{K_c}$. As temperature decreases, H_c increases. This is due to the ferromagnetic order imposed as the temperature decreases. This and the decrease of thermal activation reduces the possibility of thermally driven transitions leads to the increase of coercivity.

The coercive field varies with ${}^{K_s}/_{K_c}$. However, the system could present blocked states, or metastable states, which provide different pathways of magnetization reversal. For this reason, the exact calculation of the coercivity for an ensemble of such nanoparticles would require averaging over all paths, which is beyond the scope of the current work.

Acknowledgments

The authors gratefully acknowledge financial support from the Dirección Nacional de Investigaciones of the Universidad Nacional de Colombia during the course of this research under projects 28281 and 23088.

---

[1] M. E. Gomez, G. Campillo, J. G. Ramirez, P. Prieto, A. Hoffmann, J. Guimpel, N. Haberkorn, and A. Condó, "Magnetotransport Properties in Epitaxial Exchange-Biased La2/3Ca1/3MnO3 / La1/3Ca2/3MnO3 Superlattices," *IEEE Transactions on Magnetics*, vol. 42, no. 10, pp. 2981–2983, 2006.

[2] E. Restrepo-Parra, C. M. Bedoya-Hincapié, F. J. Jurado, J. C. Riano-Rojas, and J. Restrepo, "Monte Carlo study of the critical behavior and magnetic properties of La2/3Ca1/3MnO3 thin films," *Journal of Magnetism and Magnetic Materials*, vol. 322, no. 21, pp. 3514–3518, 2010.

[3] C. Zener, "Interaction between the d -Shells in the Transition Metals. II. Ferromagnetic Compounds of Manganese with Perovskite Structure," *Physical Review*, vol. 82, no. 3, pp. 403–405, 1951.

[4] E. Restrepo-Parra, C. D. Salazar-Enríquez, J. Londoño-Navarro, J. F. Jurado, and J. Restrepo, "Magnetic phase diagram simulation of La1-xCaxMnO3 system by using Monte Carlo,

Metropolis algorithm and Heisenberg model," *Journal of Magnetism and Magnetic Materials*, vol. 323, no. 11, pp. 1477–1483, 2011.

[5] Y. Labaye, O. Crisan, L. Berger, J. M. Greneche, and J. M. D. Coey, "Surface anisotropy in ferromagnetic nanoparticles," *Journal of Applied Physics*, vol. 91, no. 10, p. 8715, 2002.

[6] J. F. Bobo, L. Gabillet, and M. Bibes, "Recent advances in nanomagnetism and spin electronics," *Journal of Physics: Condensed Matter*, vol. 16, no. 5, pp. S471–S496, 2004.

[7] Q. A. Pankhurst, J. Connolly, J. S. K, and J. Dobson, "Applications of magnetic nanoparticles in biomedicine," *Journal of physics D: Applied Physics*, vol. 36, pp. R167–R181, 2003.

[8] P. Dey and T. K. Nath, "Effect of grain size modulation on the magneto- and electronic-transport properties of La0.7Ca0.3 MnO3 nanoparticles: The role of spin-polarized tunneling at the enhanced grain surface," *Physical Review B*, vol. 73, no. 21, p. 214425, 2006.

[9] H. Kachkachi and M. Dimian, "Hysteretic properties of a magnetic particle with strong surface anisotropy," *Physical Review B*, vol. 66, no. 17, p. 174419, 2002.

[10] H. Kachkachi and H. Mahboub, "Surface anisotropy in nanomagnets: transverse or Néel?," *Journal of Magnetism and Magnetic Materials*, vol. 278, no. 3, pp. 334–341, 2004.

[11] J. Mazo-Zuluaga, J. Restrepo, F. Muñoz, and J. Mejía-López, "Surface anisotropy, hysteretic, and magnetic properties of magnetite nanoparticles: A simulation study," *Journal of Applied Physics*, vol. 105, no. 12, p. 123907, 2009.

[12] R. Mahesh, R. Mahendiran, A. K. Raychaudhuri, and C. N. R. Rao, "Effect of particle size on the giant magnetoresistance of La0.7Ca0.3MnO3," *Applied Physics Letters*, vol. 68, no. 16, p. 2291, 1996.

[13] E. Restrepo-Parra, G. Orozco-Hernández, and J. C. Riaño-Rojas, "Monte Carlo simulation of surface anisotropy in La2/3Ca1/3MnO3 nanoparticles," *Journal of Magnetism and Magnetic Materials*, vol. 344, pp. 44–48, 2013.

[14] T. Hotta and E. Dagotto, "Theory of Manganites," in *Colossal Magnetoresistive Manganites* (T. Chatterji, ed.), vol. 1, ch. 5, pp. 207–262, Netherlands: Springer Netherlands, 1 ed., 2004.

[15] Ò. Iglesias and A. Labarta, "Influence of surface anisotropy on the hysteresis of magnetic nanoparticles," *Journal of Magnetism and Magnetic Materials*, vol. 290-291, pp. 738–741, 2005.

[16] M. Uhl and B. Siberchicot, "A first-principles study of exchange integrals in magnetite," *Journal of Physics: Condensed Matter*, vol. 7, no. 22, pp. 4227–4237, 1995.

[17] P. Schiffer, A. P. Ramirez, W. Bao, and S. W. Cheong, "Low temperature magnetoresistance

and the magnetic phase diagram of La1-xCaxMnO3," *Physical review letters*, vol. 75, no. 18, pp. 3336–3339, 1995.

[18] Ò. Iglesias and A. Labarta, "Finite-size and surface effects in maghemite nanoparticles: Monte Carlo simulations," *Physical Review B*, vol. 63, no. 18, p. 184416, 2001.

[19] E. A. Velásquez, J. Mazo-Zuluaga, J. Restrepo, and Ó. Iglesias, "Pseudocritical behavior of ferromagnetic pure and random diluted nanoparticles with competing interactions: Variational and Monte Carlo approaches," *Physical Review B*, vol. 83, no. 18, p. 184432, 2011.

[20] A. G. Kolhatkar, A. C. Jamison, D. Litvinov, R. C. Willson, and T. R. Lee, "Tuning the Magnetic Properties of Nanoparticles," *International Journal of Molecular Sciences*, vol. 14, no. 8, pp. 15977–16009, 2013.

[21] J. Sung Lee, J. Myung Cha, H. Young Yoon, J.-K. Lee, and Y. Keun Kim, "Magnetic multi-granule nanoclusters: A model system that exhibits universal size effect of magnetic coercivity," *Scientific Reports*, vol. 5, p. 12135, 2015.

[22] R. Yanes, O. Chubykalo-Fesenko, H. Kachkachi, D. A. Garanin, R. Evans, and R. W. Chantrell, "Effective anisotropies and energy barriers of magnetic nanoparticles with Néel surface anisotropy," *Physical Review B*, vol. 76, no. 6, p. 064416, 2007.

[23] X. Zianni, K. N. Trohidou, and J. A. Blackman, "Effect of surface anisotropy on the coercive field of small magnetic particles," *Journal of Applied Physics*, vol. 81, no. 8, pp. 4739–4740, 1997.

[24] L. Berger, Y. Labaye, M. Tamine, and J. M. D. Coey, "Ferromagnetic nanoparticles with strong surface anisotropy: Spin structures and magnetization processes," *Physical Review B*, vol. 77, no. 10, p. 104431, 2008.

[25] Ò. Iglesias and A. Labarta, "Role of surface disorder on the magnetic properties and hysteresis of nanoparticles," *Physica B: Condensed Matter*, vol. 343, no. 1, pp. 286–292, 2004.

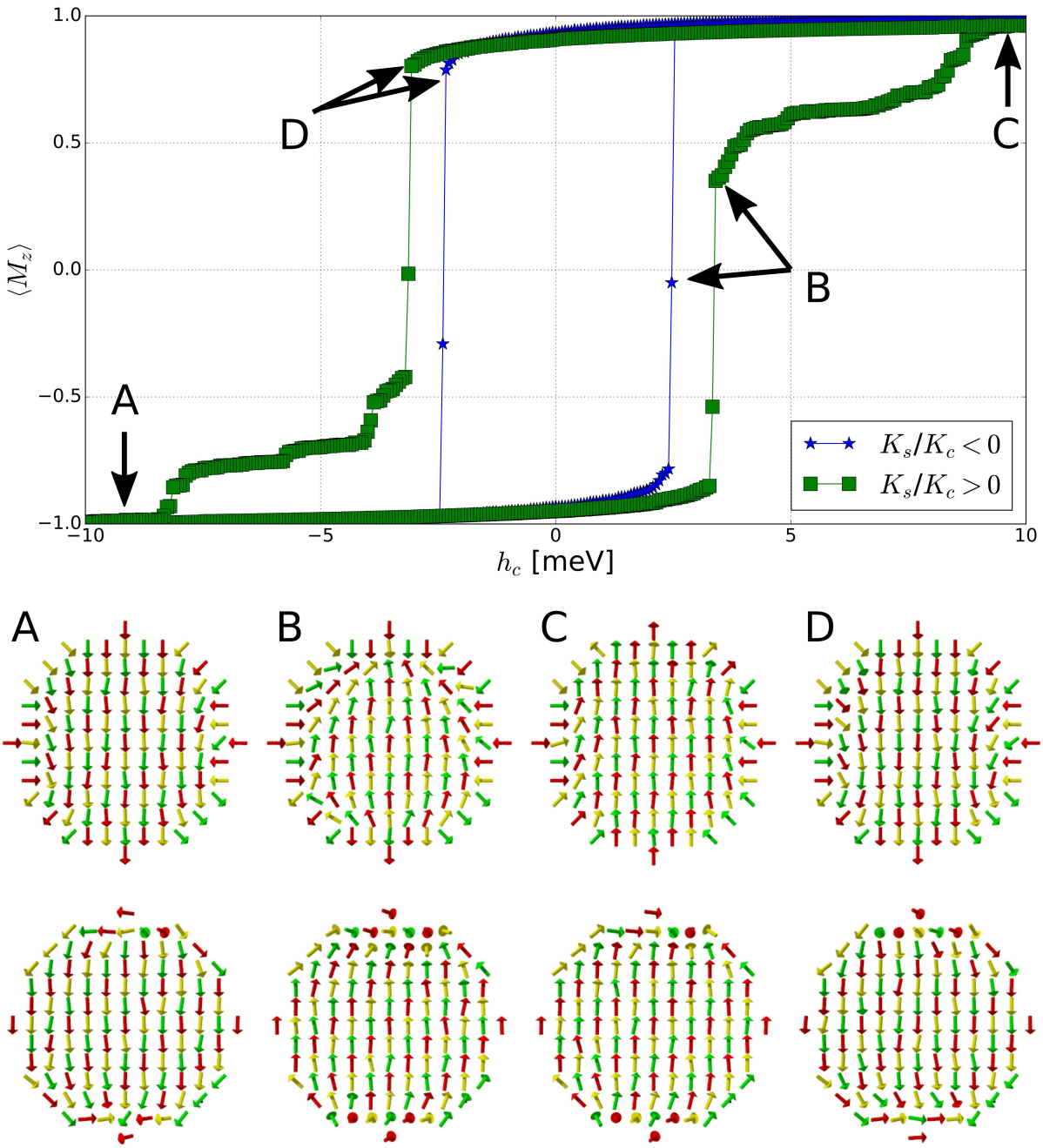

Figure 7: Hysteresis loops for a nanoparticle with $D = 12$ ions, $T = 10K$ and $^{K_s}/_{K_c} = \pm 10000$ with its respective spin configuration in the plane XZ. Upper and lower figures correspond to $K_s > 0$ and $K_s < 0$, respectively. (lines are just a guide to the eye).

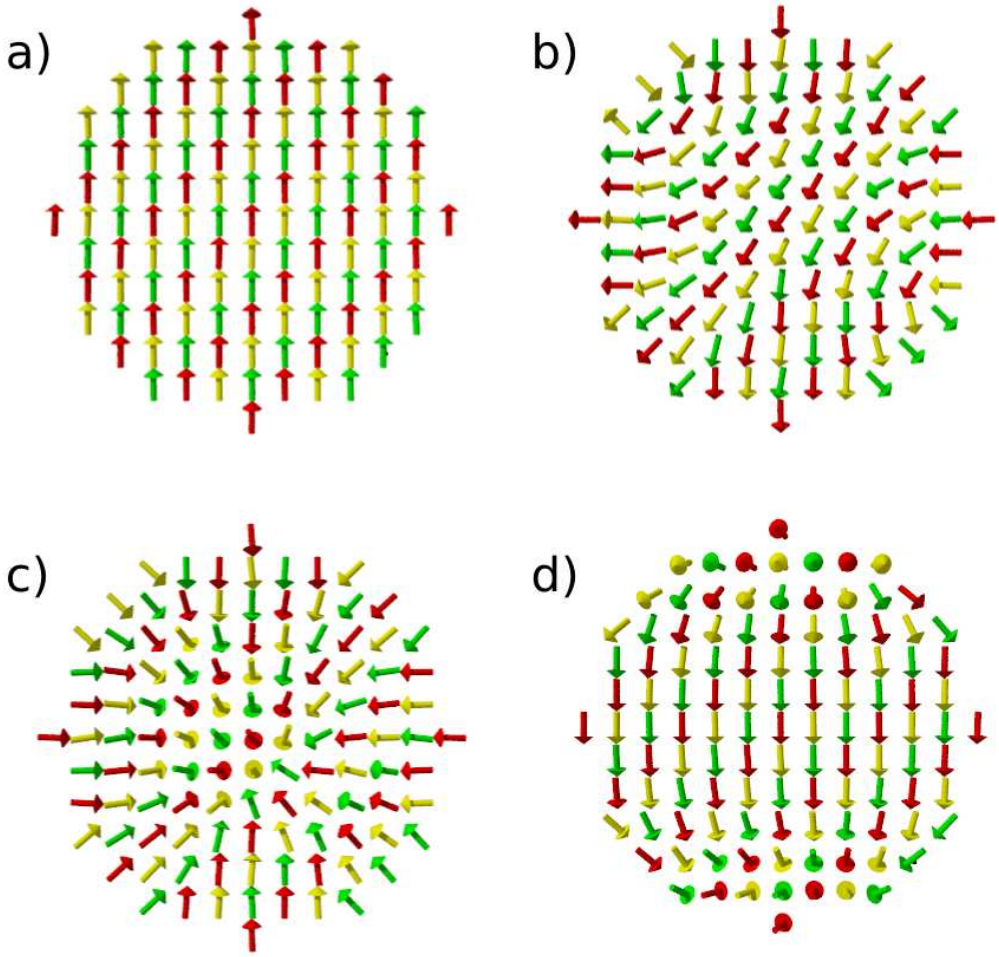

Figure 8: Spin configuration for a manganite nanoparticle of diameter $D = 12$ ions for (a) ${}^{K_s}/_{K_c} \to 0$, collinear ferromagnetic configuration, (b) ${}^{K_s}/_{K_c} = 100$, "throttled" configuration, (c) ${}^{K_s}/_{K_c} \to \infty$, "hedgehog" configuration and (d) ${}^{K_s}/_{K_c} = -100$, "artichoke" configuration.